Shell Crystallization in Granular Hopper Flow

Sheng Zhang
Institute of Modern Physics
Ping Lin
Institute of Modern Physics
Mengke Wang
Institute of Modern Physics
Jiang-Feng Wan
East China University of Technology
Yi Peng
Institute of Modern Physics
Lei Yang (lyang_imp@outlook.com)
Institute of Modern Physics
Meiying Hou
Institute of Physics

Research Article

Keywords: interesting phenomenon, crystallized shell, DEM simulation

Posted Date: March 3rd, 2021

DOI: https://doi.org/10.21203/rs.3.rs-250608/v1

Shell crystallization in granular hopper flow

Authorship

Sheng Zhang[1,2,*], Ping Lin[1,2,*], Mengke Wang[1,2], Jiang-feng Wan[3], Yi Peng[1,2], Lei Yang[1,2,4,✉], Meiying Hou[2,5,✉]

[1] Institute of Modern Physics, Chinese Academy of Sciences, Lanzhou, 730000, China
[2] University of Chinese Academy of Sciences, Beijing, 100049, China
[3] East China University of Technology, Nanchang, 330105, China
[4] Lanzhou University, Lanzhou, 730000, China
[5] Institute of Physics, Chinese Academy of Sciences, Beijing, 100190, China

*Zhang S and Lin P contributed equally to this work.
✉Correspondence and requests for materials should be addressed to Hou M (email: mayhou@iphy.ac.cn) or to Yang L (email: lyang_imp@outlook.com)

Abstract

An interesting phenomenon that a layer of crystallized shell formed at the container wall during hopper flow is observed experimentally and is investigated in DEM simulation. Different from shear or vibration driven granular crystallization, our simulation shows during the hopper flow the shell layer is formed spontaneously from the stagnant zone at the base and grows at a constant rate to the top with no external drive. The growth rate of the shell is found linearly proportional to the rate of the hopper flow. This shell is static and served as a new wall, which changes the flow profiles and its stress properties, and in turn guarantees a constant flow rate.

Introduction

Self-organized ordering widely appears in nature, from ripples in sand, waves of the sea, to the spirals on the shell of snails and the bacterial snowflakes [1-4]. Ordering phenomena are also widely studied in driven disordered system [5-8]. As a non-equilibrium model system, agitated granular matter has often been used in the lab to study the mechanisms behind these ordering phenomena. Particle alignment, related to ordering, rheology and entropy in disordered systems, has frequently been induced and investigated in shearing, twisting, shaking or inclined-flow granular media [7, 9-11]. Different from these external agitations induced granular ordering, we report in this work

observation of a layer of shell crystallized spontaneously at the container wall during hopper flow without external agitation.

Hopper flow of granular material is featured by its constant flow rate. The flow rate can be described by Beverloo's scaling law quantitatively: $W = C\,\rho\,\sqrt{g}\,(D_0 - kd_0)^{2.5}$, where D_0 denotes the outlet size, ρ is the apparent density of the granular material and g is the gravitational acceleration. C and k are empirical constants which depend on the grain and container properties, such as friction coefficients, particle shape or hopper angle [12-14]. The constancy of the flow rate may be related to either the dynamical Janssen effect or the existence of a 'free fall arch' region [15] over the outlet. Continuum modeling of hopper-flow by Staron et al. successfully reproduced the constant flow rate and pressure cavity by implementing a plastic rheology in the Navier-Stokes solver [16]. These findings imply that when discharging from a hopper, granular material resembles other visco-plastic fluids with a shear stress changing from shear rate γ-independent in the elastic limit to $\sim\gamma^2$ in rapid shear flow [17] as described by Bagnold already in 1954 [18]. Several recent studies focused on the frictional properties of the particles and the silo wall which are crucial in setting the flow profile and the flow rate. Experimental observations by X-ray tomography [19] or electrical capacitance tomography [20] showed, that increasing wall roughness leads to increasing thickness of the shear zone near the wall for sand. Similarly, DEM simulations by Gonzalez show that increasing wall roughness leads to a mass flow-funnel flow transition [21]. The discharge rate of a silo was reported to systematically decrease with increasing the surface roughness of the particles [22] or with increasing internal angle of friction of the granular material [23]. In the DEM simulations by Vidyapati the discharge rate decreased with increasing interparticle friction, but was insensitive to the wall friction [24].

In this work we report a peculiar phenomenon observed in experiment and investigated in simulation, that during the drainage a crystallized granular shell develops next to the wall. The development of the shell gradually changes the flow profile inside the silo as it leads to a change in the friction at the boundary without changing the interparticle friction in the bulk. We explore the process leading to the formation of the shell and analyze whether it influences the flow rate of the silo. The development of crystalline ordering was reported in other (sheared or shaken) granular systems before [6, 10, 25-28], where the volume fraction and particle-particle friction played an important role. The initial crystallized 'nucleus' appeared not only at the boundary but also in the central region [10, 29]. Other examples, such as for inclined flow under gravity, the ordering arises upon ordered base or driven by the side wall friction [11, 30]. Our observation of the remaining crystallized granular shell also reminds for comparison with the slow motion of retention of viscous fluid on a vertical plate as investigated by Jeffreys in 1930 [31] and by Gutfinger and Tallmadge [32] in non-Newtonian fluids. Compared to fluids, there are two major differences in the granular case: 1) the formation of a crystallized shell is a dynamical process grown upwards from bottom; 2) the crystallized shell in our case grows during the drainage and is still mechanically stable after drainage.

Results and Discussions

Formation of the shell

Figure 1 The simulation system with a cylindrical coordinates system. The origin is set at the center of the bottom.

Crystallized shells of particles next to the wall during hopper drainages are both observed in our experiments and simulations (shown in Video 1, Video 2 and Video 3). Numerical simulation investigates the dynamics of the shell formation and its influencing factors in a cylindrical hopper with a flat bottom (see Figure 1). In order to describe the growth of crystallized shells, three types of particles are defined here as one gets closer to the wall: ***boundary particle***, if its radial coordinate is greater than $D/2\text{-}d_0$; ***wall particle***, if the particle touches the sidewall (i.e., radial coordinate is equal to or greater than $D/2\text{-}r_0$), and ***shell particle***, which is a wall particle touching six neighboring wall particles to form a nearly static crystallized shell. To define the top surface of the shell, the boundary layer (all the particles with an r-coordinate larger than $D/2\text{-}d_0$) is divided into several vertical columns. In each column the shell particles are recognized from bottom to top. The last shell particle in this column is defined as the shell particle k when there is no other shell particle located in the range (z_k, z_k+20d_0), where z_k is the z coordinate of particle k.

After starting the flow, local configuration of packing close to the sidewall will self-organize into ordered state. The participating particles come from the boundary particles of the initial packing (see in Figure 2a, Figure S3). Each particle in ordered state touches six neighboring wall particles to form a crystallized shell. This stable crystallized configuration initially appears at the bottom and then grows upwards. It takes several seconds for the crystallized shell to spread and reach the

descending level. Usually, the shell is not a perfect hexagonal cell. It is divided into some "mono-crystalline" cells with boundaries between them [10], which are shown in Figure 2c (also shown in Video 1).

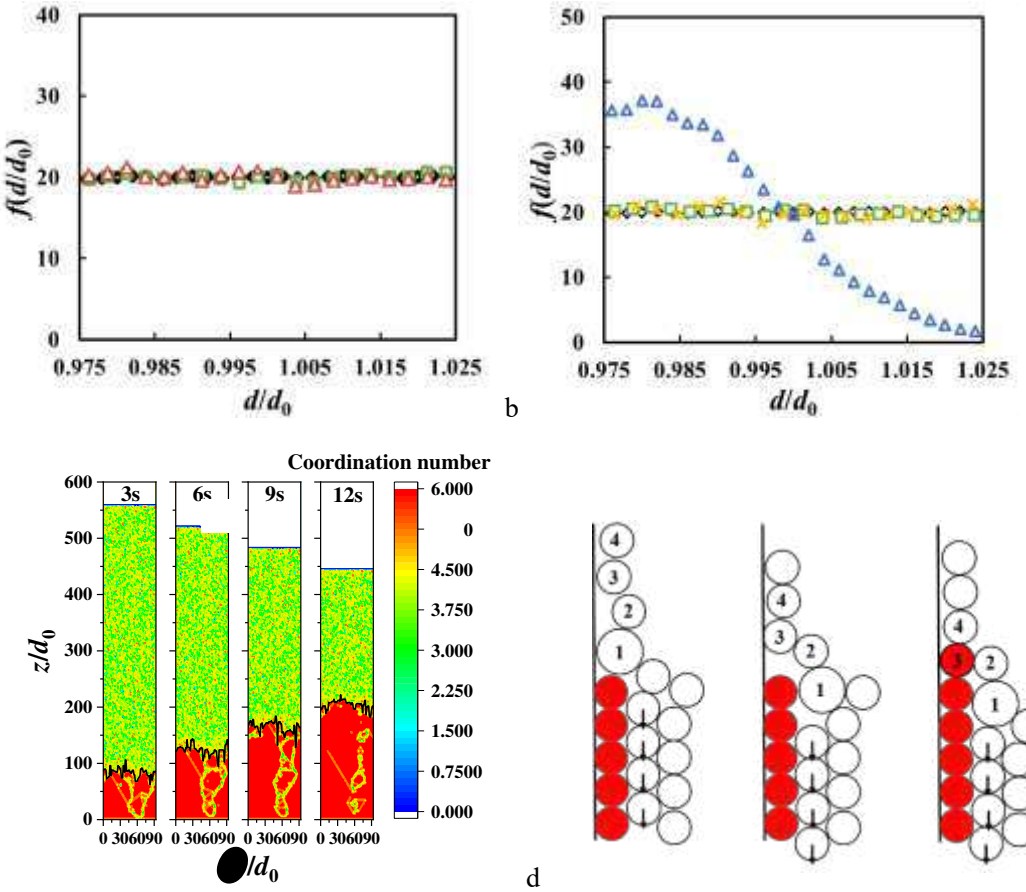

Figure 2 a) Frequency distribution of the initial radial coordination of shell particles. Size distribution of different particle groups with a) μ_{pp}=0.5; b) μ_{pp}=0.05. Diamond(black): all particles in the hopper. Square(green): particles at the boundary when the flow starts. Upper triangle(blue): the shell particles when the drainage is over. x(yellow): the boundary particles above the upper surface during the drainage. Upper triangle(red): the boundary particles when flow is stable. c) Side area of the cylindrical hopper at different time (3, 6, 9, 12s after the flow starts), showing the growth of the crystallized shell. The color denotes the coordination number of wall particles. The red particles are shell particles. Black lines denote the local surface of the shell. d) Illustration of the shell growth. The red particles denote the shell particles. The proper size particle (particle 3) is selected by settling down process while particles 1 and 2 flow aside.

Smaller μ_{pp} helps to generate more wall particles to enforce the growth of the crystallized shell. Besides friction, as mentioned above, dispersity is known as another important factor for shear-induced ordering [8, 33]. Our simulations also show that the distribution of particle size does influence the formation of the crystallized shell. The shell does not form when the global dispersity λ is large (0.1 for instance). A small λ guarantees the mechanical stabilization of the shell after the drainage. Figure 2b shows the size distribution in the crystallized shell. The dispersity in the shell is less than the global dispersity, which reveals segregation taking place during the drainage.

The shell growth is schematically illustrated in Figure 2d. The already existing shell particles can be considered as the substrate during a crystal growth process. The wall particles flow downwards with a motion involving sliding and rotation [34] in contact with the wall, . This process depends on the local configurations of the flowing region just above the top of the shell. The height of this region is about 2-3d_0 as the motions of wall particles will be affected by inner particles. The main ingredient of this selection process is that the shell 'prefers' to choose the particle that has about the same size (see in Figure 2b), which leads to the narrower dispersity in the shell particles. This follows from the fact, that a narrower size dispersity helps to mechanically stabilize the shell.

Growth rate

Table 1 Growth rate of the shell v_s. Here λ=0.

μ_{pw}	0.0	0.05	0.1	0.2	0.5	0.1			
μ_{pp}	0.05					0.0	0.01	0.05	0.1
Grow rate v_s (d_0/s)	26.3	26.2	25.9	24.5	22.9	76.0	58.8	25.9	12.6

The local surface height of shell $\bar{h}(t)$ is averaged for every snapshot and every column (see Figure 3a). We see, that the growth of the averaged surface height is nearly linear except at initial stage when the base of the shell is forming. During that stage there is no selection and only rearrangement is permitted, since the particles near the bottom of the hopper are stagnant. The slope of the linear region is defined as growth rate of the shell v_s. The growth rate v_s with varying μ_{pp} and μ_{pw} are shown in Table 1. It drops from v_s=76.0 d_0/s when μ_{pp}=0 to 12.6 as μ_{pp} grows to 0.1. The crystallized shell is no longer observed if μ_{pp} exceeds 0.1. It is also found that the friction between particles and sidewall μ_{pw} has a minor effect to the formation of the shell.

In analogy to the model of crystal growth [35], it is natural to associate the particle velocity to the growth rate. Since the flowing particles above the surface of the shell have nearly the same velocity, the velocity of potential shell particles can be calculated as: $v_p \approx \frac{\varphi}{\rho_b A}$, where φ flow rate, ρ_b bulk density of hopper flow and $A = \pi D^2/4$ is the cross area of the hopper. We found that for each hopper size, there is a linear relationship between v_s and v_p (Figure 3b). With small hopper size D, the slope of this dependence seems to have a limit value of 7. When $D \geq 30d_0$, the slope ~ D^{-1} (Figure 3c). It is not checked here if the slope will drop to zero when D further increases.

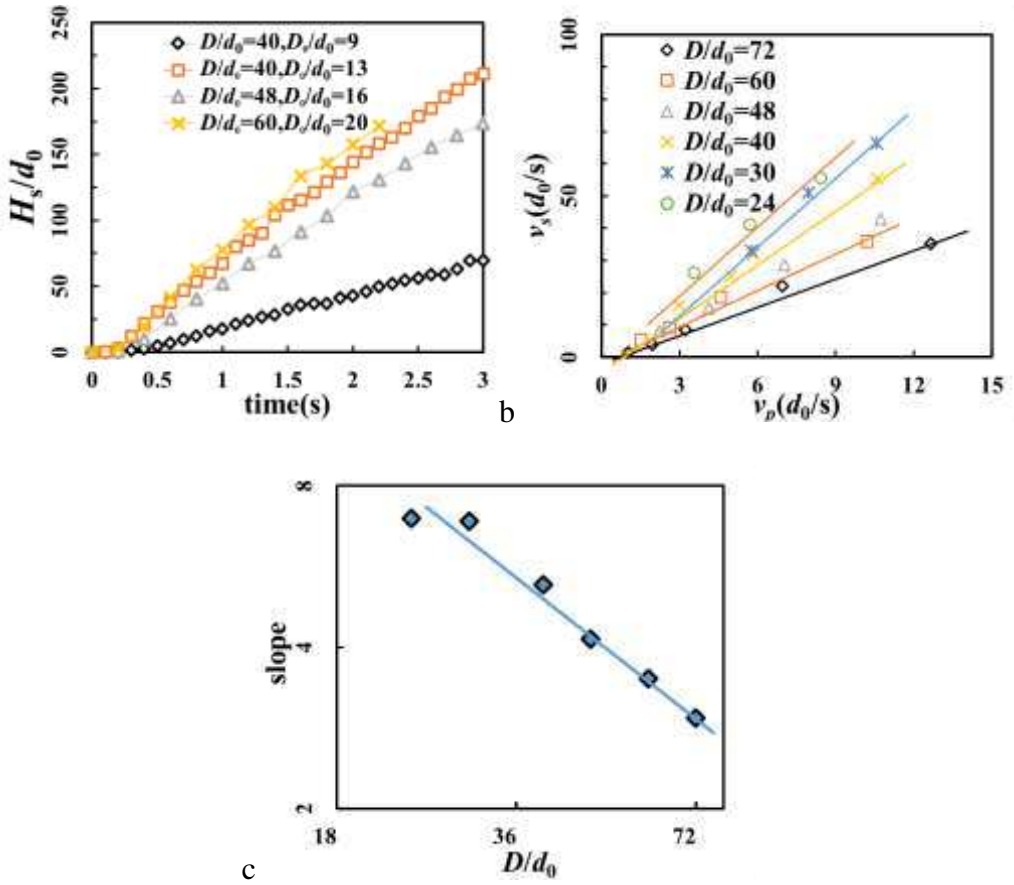

Figure 3 a) The development of averaged shell surface height (H_s) with different D and D_0. b) The relation between v_p and v_s. c) Log-log plot of the slope of the linear relationship presented in Figure 4b. Here λ=0.

Shear layers

Our simulations show that the growth of the crystallized shell is dominated by two parameters, the sliding friction coefficient μ_{pp} and the global dispersity of particles λ. In this section, three cases with different μ_{pp} and λ are presented for comparison while μ_{pw} is fixed to be 0.1 (see Table 2): case A: μ_{pp}=0.05 and λ=0; case B: μ_{pp}=0.5 and λ=0, and case C: μ_{pp}=0.05 and λ=0.1. We see crystallized shell only in case A, but not in cases B and C.

Table 2 Parameters in 6 cases.

Cases	A	B	C	A*	B*	C*
μ_{pp}	0.05	0.5	0.05	0.05	0.5	0.05
μ_{pw}	0.1	0.1	0.1	0	0	0
λ	0	0	0.1	0	0	0.1

In case A, the wall particles are rearranged into hexagonal ordered state after flow begins. The value of local orientational order q_6 is above 0.55, which is higher than that in the central region (0.45 is

a typical value for disordered packing [36]) (see Figure 4).Compared to the cases without crystallized shell (case B and case C), the shear rate in the shear layers is obviously higher in case A. Due to the shear, the granular temperature for particles in the shear layers is higher than in the central region, which is also the case seen in inclined flow [37]. The volume fraction close to the sidewall is slightly smaller in case B, which is consistent with the local high temperature [38]. When λ is 0.1 (case C), a plug-like flow occurs and v_z is much larger than in cases A and B. Both the shear rate and the granular temperature are then close to zero.

It is interesting that during the growth of the crystallized shell, there are two coexisting phases of the flow (see Figure 5). In the area where the crystallized shell has formed, the ordered wall particles are nearly static, and shear is concentrated near the shell. Above this area where the crystallized shell is not developed yet, v_z of all particles is still nearly uniform and no obvious shear layer is observed. Thus, the occurrence of shear layers is due to this crystallization. The shear flow region expands upwards until the growing crystallized shell encounters the top surface of the descending level. In our simulation, funnel flow is not observed even if μ_{pp} reaches 0.5, perhaps because the wall friction is not enough here [39]. The crystallized shell remains static after the drainage, which is found in our experiment (see Figure S2 and Video 2). Moreover, the growth rate is measured and the value is 7.42±0.53 d_0/s, which is less than that in simulations.

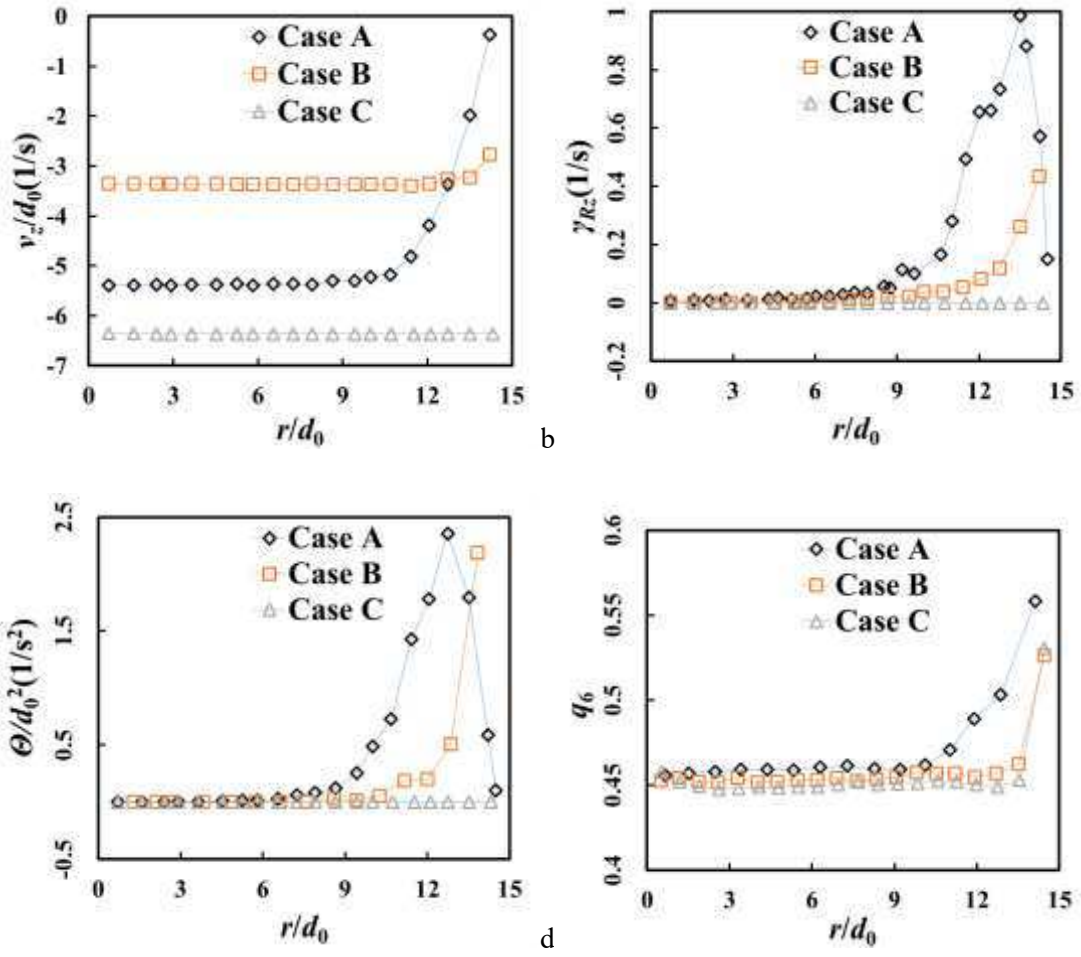

Figure 4 Radial profiles of a) vertical velocity v_z, b) shear rate, c) granular temperature, d)

orientational order q_6 at z=100 d_0.

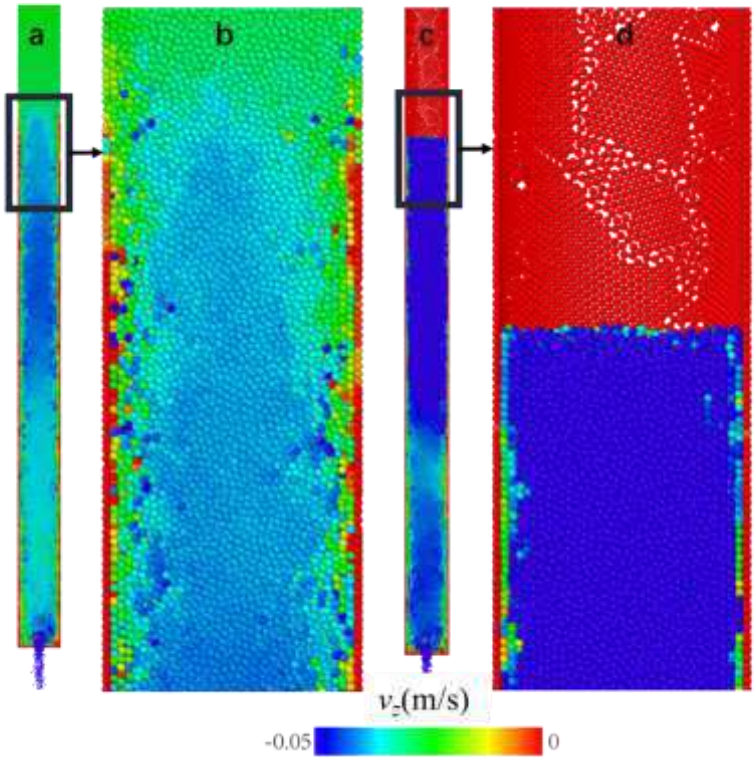

Figure 5 a) A cross section of the flow at a stage when the crystallized shell does not reach the descending top surface. b) Enlarged picture of the part around the growing shell surface in a). c) The cross section of the flow when the top surface level is below the shell surface. d) Enlarged picture of the part around the top surface in c), with the developed shell reaching well above the surface. The results in this figure is visualized by [40].

Compared with the reported crystallizations mentioned above [7, 9, 10], the phenomenon found in our case is however different. First of all, the hopper wall in our case is vertical and smooth. The mechanical stability of the crystallized shell is supported by the bottom and where the shell is formed, it is like a frictional wall, leading to strong shear in the neighboring layers. Therefore as shown in Figure 6a, a Janssen-like stress profile still exists in a frictionless hopper, similar to the one observed in the normal frictional hoppers [41, 42]. As the weight of particles is supported by the shell, there is a strong peak of vertical stress at the boundary (see in Figure 6c). For comparison, when λ=0.1, σ_{zz} behaves like hydrostatic pressure, which is linear with height except near the bottom (Figure 6b).

The variations of instantaneous flow rates with time are shown in Figure 6d. In previous DEM simulations, the flow rate will decrease with time by inducing a small wall friction [41, 43]. Interestingly, the results show that the flow rate is constant with the growing crystallized shell (Case A*) and decreases in the situation without the shell (Case C*), which questions the relationship between the flow rate and the roughness (or friction) of sidewalls. The flow rate in Case B* is smaller than that in both of Cases A* and C*, which verifies the influence of particle-particle friction reported in previous studies [22, 23].

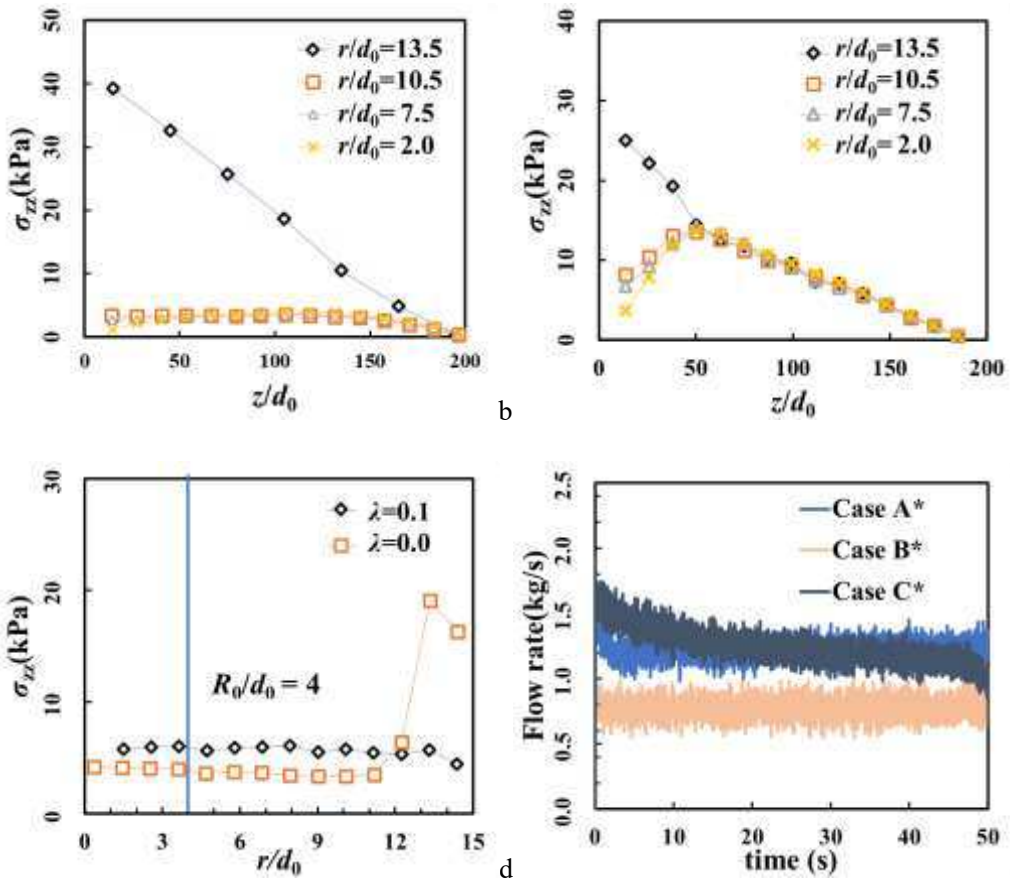

Figure 6 Vertical stress σ_{zz} along z axis in a) Case A* (λ=0) and b) in Case C* (λ=0.1) (see Table 2). c) σ_{zz} in the radial direction at z/d_0 =100. The vertical line marks the radius of outlet. d) Temporal profile of instantaneous mass flow rate in Cases A*, B* and C*.

Conclusion

We have investigated numerically of the experimental observation that a layer of crystallized shell formed at the container wall during the hopper flow. Our simulation shows the degree of the particle polydispersity and particle-particle friction are two main factors to prevent the shell formation. Those particles being pushed to the wall by the flowing particles, tend to pile up from the base and grow to the top during the flow. The faster the flow rate is, the faster the growth rate of the shell layer piles. The ratio of the rates depends on the container diameter. The smaller the container the larger the ratio is. Once it is formed, the shell remains there, even when the flow ends. This formed shell serves as a new wall, which guarantees the flow rate constant no matter what wall material is. This phenomenon is interesting not only for its formation of crystallized shell with no need of external drive, but also for its altering the flow properties and stabilizing the flow rate.

Methods

Simulation method

To model the dynamical behavior of particles, our simulations are carried out on multiple GPUs using the DEM code (Discrete Element Method) developed by us [44]. DEM is a widely used simulation tool in granular mechanics, in which particle positions, velocities and interactions are tracked by equations of motion, simple contact models being then provided. In our simulation, the soft-particle contact model is used where the interactions consisting of elastic and viscous components in normal and tangential directions are calculated from the overlap and its time rate of change. By the Hertz-Mindlin contact model [45, 46], the normal and tangential contact forces between two contacting particles are:

$$\begin{cases} \boldsymbol{F}_{ij_n} = \frac{4}{3} Y_{\text{eff}} \sqrt{R_{\text{eff}} \delta_{ij_n}} \boldsymbol{\delta}_{ij_n} - 2\sqrt{\frac{5}{6}} \beta \sqrt{2 Y_{\text{eff}} \sqrt{R_{\text{eff}} \delta_{ij_n}} m_{\text{eff}}} \boldsymbol{v}_{ij_n} \\ \boldsymbol{F}_{ij_t} = 8 G_{\text{eff}} \sqrt{R_{\text{eff}} \delta_{ij_n}} \boldsymbol{\delta}_{ij_t} - 2\sqrt{\frac{5}{6}} \beta \sqrt{8 G_{\text{eff}} \sqrt{R_{\text{eff}} \delta_{ij_n}} m_{\text{eff}}} \boldsymbol{v}_{ij_t} \end{cases} \tag{1}$$

$$\beta = \frac{\ln e}{\sqrt{\ln^2 e + \pi^2}} \tag{2}$$

$$Y_{\text{eff}} = 1/((1-\nu_i^2)/Y_i + (1-\nu_j^2)/Y_j) \tag{3}$$

$$G_{\text{eff}} = 1/(2(2+\nu_i)(1-\nu_i)/Y_i + 2(2+\nu_j)(1-\nu_j)/Y_j) \tag{4}$$

$$r_{\text{eff}} = r_i r_j/(r_i + r_j) \tag{5}$$

$$m_{\text{eff}} = m_i m_j/(m_i + m_j) \tag{6}$$

where G is the shear modulus, Y is the Young's Modulus, r is the radius of the particles, m is the mass of particles and e is the coefficient of restitution between particles. $\boldsymbol{\delta}_{ij\text{n}}$ and $\boldsymbol{\delta}_{ij\text{t}}$ are normal and tangential displacement vectors, and $\delta_{ij\text{n}}$ and $\delta_{ij\text{t}}$ are their modules, respectively. $\mathbf{v}_{ij\text{n}}$ and $\mathbf{v}_{ij\text{t}}$ are normal and tangential relative velocities between the particles i and j. $\boldsymbol{\delta}_{ij\text{n}} \equiv (R_i + R_j - r_{ij})\mathbf{r}_{ij}/r_{ij}$ and $\delta_{ij\text{t}}$ is determined by integrating $\mathbf{v}_{ij\text{t}}$. Considering sliding friction, the Coulomb yield criterion $F_{ij\text{t}} \leq \mu_s F_{ij\text{n}}$ is satisfied by truncating tangential overlap $\mathbf{u}'_{ij} = \mu_s F_{ij\text{n}} \mathbf{u}_{ij}/F_{ij\text{t}}$ [46]. μ_s is the sliding friction coefficient between particles. $\mathbf{u}'_{ij}$ and $\mathbf{u}_{ij}$ are truncated and original tangential overlap respectively. Further more, rolling and torsion friction should be introduced for irregular shaped particles. These influences are given by rolling and torsion torques:

$$\begin{cases} \boldsymbol{M}_r = -\mu_r F_{ij_n} \hat{\boldsymbol{\omega}}_{ij} \\ \boldsymbol{M}_t = -\mu_t F_{ij_n} \hat{\boldsymbol{\omega}}_{ij} \end{cases} \tag{7}$$

μ_r and μ_t are rolling and torsion frictions respectively, $\hat{\boldsymbol{\omega}}_{ij}$ is the relative angular velocity between two contacting particles.

Under gravity field, the equations of motion of the particles are:

$$\begin{cases} m_i \boldsymbol{a}_i = \sum_j \left(\boldsymbol{F}_{ij_n} + \boldsymbol{F}_{ij_t} \right) + m_i \boldsymbol{g} \\ I_i \dot{\boldsymbol{\omega}}_i = \sum_j \left[-\frac{r_i}{r_{ij}} \boldsymbol{r}_{ij} \times \left(\boldsymbol{F}_{ij_n} + \boldsymbol{F}_{ij_t} \right) \right] \end{cases} \tag{8}$$

These equations are solved by integration using the Velocity-Verlet scheme [47]. The model parameters used in our simulations are listed in Table 3.

Table 3 Case parameters in simulations

Physical Quantity	**Symbol**	**Value**
Averaged particle diameter	d_0	6.0 mm
Global dispersity	λ	0.0, 0.05, 0.1
Particle density	ρ	2850 kg/m^3
Elastic modulus	Y	72 GPa
Poisson's ratio	v	0.25
Particle-particle friction coefficient	μ_{pp}	0, 0.01, 0.05, 0.1, 0.5
particle-wall friction coefficient	μ_{pw}	0, 0.05, 0.1, 0.2, 0.5
Particle-particle and particle-wall coefficient of restitution	e	0.6
Particle-particle and particle-wall rolling friction coefficient	μ_r	1 mm
Particle-particle and particle-wall torsion friction coefficient	μ_t	0.4 mm
Outlet diameter	D_0	8 d_0
Hopper diameter	D	30 d_0

Definitions of quantities

The size distribution of particles in the simulation is uniform in the rage $((1-1/2\lambda)d_0, (1+1/2\lambda)d_0)$, where λ is named to be the global dispersity of particles. The local orientational factor q_6 [48, 49] and the granular temperature [50] are calculated in our system. The q_6 of the i-th particle is given by:

$$q_6 = \left[\frac{4\pi}{13}\sum_{m=-6}^{6}\left|\bar{Q}_{6m,i}\right|^2\right]^{1/2} , \tag{9}$$

where $\bar{Q}_{6m,i} = \frac{1}{N_i}\sum_j^i Q_{6m}(\vec{r}_{ij})$, and $\vec{r}_{ij}$ is the midpoint between particle i and j, Q_{6m} is spherical harmonics Y_{lm} when l=6. In our simulation, granular temperature in z direction is given by:

$$\Theta = \langle v_z^2\rangle - \langle v_z\rangle^2 \tag{10}$$

The bracket denotes an average value of particle velocities within a volume Ω. $\langle v_z\rangle$ is the corresponding local average vertical velocity. The stress is calculated by virial stress[51]:

$$\sigma_{\alpha\beta} = \frac{1}{\Omega}\sum_{i\ in\ \Omega}\left(-m^i\left(v_\alpha^i - \overline{v_\alpha}\right)\left(v_\beta^i - \overline{v_\beta}\right) + \frac{1}{2}\sum_j\left(x_\alpha^j - x_\alpha^i\right)f_\beta^{ij}\right) \tag{11}$$

where m^i is the mass of the i-th particle in a volume Ω , x_α^j its position with Cartesian components, v_α^i its velocity, $\overline{v_\alpha}$ the local average velocity, and f_α^{ij} is the force on molecule exerted by another particle.

The shear rate is given by:

$$\Gamma_{\alpha\beta} = \Delta\langle v_\alpha \rangle / \Delta L_\beta \quad (12)$$

$\langle v_\alpha \rangle$ is the average velocity of particles in a cell along α direction, and ΔL_β is the cell size along the β direction.

Experiment setup

In the experiment (shown in Figure S1), spherical glass particles and steel particles are used with the diameter of 6±0.02mm. The cylindrical hoppers with flat bottom are made of two materials: transparent plexiglass and steel. Both diameters of the hoppers are 100mm and the openings at the bottom center have a diameter of 32mm. The experimental facility is fixed on a damping platform. The environment temperature is 21℃ with a relative humidity is 35%.

Before the experiments, the hopper is set upright vertically with blocked opening, and particles are filled up to the height of 1500mm. A high-speed camera is fixed on a tripod to shoot videos of the particles close to the wall at a frame rate of 100fps.

Acknowledgement

This work is support by the National Natural Science Foundation of China (Grant No. U1738120, 11705256 and 11905272) and the Strategic Priority Research Program of the Chinese Academy of Sciences (Grant No. XDA21010202). We thank professors T. Borzsonyi, E. Somfai and R. Blumenfeld for inspiring discussions on the issue.

Author contributions

SZ, MH and LY suggested the study. SZ designed the numerical experiment and PL ran the code. PL, SZ and MW did the numerical analysis. MW, JFW and YP did the experiments. SZ and PL wrote the manuscript. MH and LY contributed to the writing.

Competing interests

The authors declare no competing financial interests.

Reference

1. Ball, P., *The self-made tapestry : pattern formation in nature*. 1999, Oxford ; New York: Oxford University Press. vi, 287 p.
2. Kauffman, S.A., *The origins of order : self-organization and selection in evolution*. 1993, New York: Oxford University Press. xviii, 709 p.
3. Coco, G. and A.B. Murray, *Patterns in the sand: From forcing templates to self-organization.* Geomorphology, 2007. **91**(3-4): p. 271-290.
4. Lushi, E., H. Wioland, and R.E. Goldstein, *Fluid flows created by swimming bacteria drive self-organization in confined suspensions.* Proceedings of the National Academy of Sciences of the United States of America, 2014. **111**(27): p. 9733-9738.
5. Dux, C. and H. Versmold, *Light diffraction from shear ordered colloidal dispersions.* Physical Review Letters, 1997. **78**(9): p. 1811-1814.
6. Tsai, J.C., G.A. Voth, and J.P. Gollub, *Internal granular dynamics, shear-induced crystallization, and compaction steps.* Physical Review Letters, 2003. **91**(6).
7. Asencio, K., et al., *Experimental Study of Ordering of Hard Cubes by Shearing.* Physical Review Letters, 2017. **119**(22).
8. Lee, J., et al., *Unraveling the Role of Order-to-Disorder Transition in Shear Thickening Suspensions.* Physical Review Letters, 2018. **120**(2): p. 5.
9. Carvente, O. and J.C. Ruiz-Suarez, *Crystallization of confined non-Brownian spheres by vibrational annealing.* Physical Review Letters, 2005. **95**(1).
10. Panaitescu, A., K.A. Reddy, and A. Kudrolli, *Nucleation and Crystal Growth in Sheared Granular Sphere Packings.* Physical Review Letters, 2012. **108**(10).
11. Silbert, L.E., et al., *Boundary effects and self-organization in dense granular flows.* Physics of Fluids, 2002. **14**(8): p. 2637-2646.
12. Nedderman, R.M., et al., *The Flow of Granular-Materials .1. Discharge Rates from Hoppers.* Chemical Engineering Science, 1982. **37**(11): p. 1597-1609.
13. Janda, A., I. Zuriguel, and D. Maza, *Flow Rate of Particles through Apertures Obtained from Self-Similar Density and Velocity Profiles.* Physical Review Letters, 2012. **108**(24).
14. Koivisto, J. and D.J. Durian, *The sands of time run faster near the end.* Nature Communications, 2017. **8**.
15. Brown, R.L., *Minimum Energy Theorem for Flow of Dry Granules through Apertures.* Nature, 1961. **191**(478): p. 458-&.
16. Staron, L., P.Y. Lagree, and S. Popinet, *The granular silo as a continuum plastic flow: The hour-glass vs the clepsydra.* Physics of Fluids, 2012. **24**(10).
17. Campbell, C.S., *Granular material flows - An overview.* Powder Technology, 2006. **162**(3): p. 208-229.
18. Bagnold, R.A., *EXPERIMENTS ON A GRAVITY-FREE DISPERSION OF LARGE SOLID SPHERES IN A NEWTONIAN FLUID UNDER SHEAR.* Proceedings of the Royal Society of London Series a-Mathematical and Physical Sciences, 1954. **225**(1160): p. 49-63.
19. Grudzien, K., et al., *Quantitative estimation of volume changes of granular materials during silo flow using X-ray tomography.* Chemical Engineering and Processing-Process Intensification, 2011. **50**(1): p. 59-67.

20. Niedostatkiewicz, M., et al., *Application of ECT to solid concentration measurements during granular flow in a rectangular model silo.* Chemical Engineering Research & Design, 2010. **88**(8a): p. 1037-1048.
21. Gonzalez-Montellano, C., F. Ayuga, and J.Y. Ooi, *Discrete element modelling of grain flow in a planar silo: influence of simulation parameters.* Granular Matter, 2011. **13**(2): p. 149-158.
22. Sukumaran, B. and A.K. Ashmawy, *Influence of inherent particle characteristics on hopper flow rate.* Powder Technology, 2003. **138**(1): p. 46-50.
23. Tian, T., et al., *Discrete and continuum modeling of granular flow in silo discharge.* Particuology, 2018. **36**: p. 127-138.
24. Vidyapati, V. and S. Subramaniam, *Granular Flow in Silo Discharge: Discrete Element Method Simulations and Model Assessment.* Industrial & Engineering Chemistry Research, 2013. **52**(36): p. 13171-13182.
25. Alam, M. and S. Luding, *First normal stress difference and crystallization in a dense sheared granular fluid.* Physics of Fluids, 2003. **15**(8): p. 2298-2312.
26. Daniels, K.E. and R.P. Behringer, *Hysteresis and competition between disorder and crystallization in sheared and vibrated granular flow.* Physical Review Letters, 2005. **94**(16): p. 4.
27. Reis, P.M., R.A. Ingale, and M.D. Shattuck, *Crystallization of a quasi-two-dimensional granular fluid.* Physical Review Letters, 2006. **96**(25).
28. Shinde, D.P., A. Mehta, and G.C. Barker, *Shaking-induced crystallization of dense sphere packings.* Physical Review E, 2014. **89**(2): p. 6.
29. Watanabe, K. and H. Tanaka, *Direct observation of medium-range crystalline order in granular liquids near the glass transition.* Physical Review Letters, 2008. **100**(15).
30. Mandal, S. and D.V. Khakhar, *Sidewall-friction-driven ordering transition in granular channel flows: Implications for granular rheology.* Physical Review E, 2017. **96**(5).
31. Jeffreys, H., *The draining of a vertical plate.* Proceedings of the Cambridge Philosophical Society, 1930. **26**: p. 204-205.
32. Gutfinger, C. and J.A. Tallmadge, *FILMS OF NON-NEWTONIAN FLUIDS ADHERING TO FLAT PLATES.* Aiche Journal, 1965. **11**(3): p. 403-+.
33. Tsai, J.C. and J.P. Gollub, *Slowly sheared dense granular flows: Crystallization and nonunique final states.* Physical Review E, 2004. **70**(3): p. 13.
34. Louge, M.Y. and S.C. Keast, *On dense granular flows down flat frictional inclines.* Physics of Fluids, 2001. **13**(5): p. 1213-1233.
35. Edwards, S.F. and D.R. Wilkinson, *The Surface Statistics of a Granular Aggregate.* Proceedings of the Royal Society of London Series a-Mathematical Physical and Engineering Sciences, 1982. **381**(1780): p. 17-31.
36. Aste, T., et al., *Investigating the geometrical structure of disordered sphere packings.* Physica a-Statistical Mechanics and Its Applications, 2004. **339**(1-2): p. 16-23.
37. Silbert, L.E., J.W. Landry, and G.S. Grest, *Granular flow down a rough inclined plane: Transition between thin and thick piles.* Physics of Fluids, 2003. **15**(1): p. 1-10.
38. Ahn, H. and C. Brennen, *Channel flows of granular materials and their rheological implications*, in *Particulate Two-Phase Flow*, M.C. Roco, Editor. 1993, Butterworth-Heinemann. p. 210-243.
39. Yu, Y.W. and H. Saxen, *Discrete element method simulation of properties of a 3D conical hopper with mono-sized spheres.* Advanced Powder Technology, 2011. **22**(3): p. 324-331.

40. Stukowski, A., *Visualization and analysis of atomistic simulation data with OVITO–the Open Visualization Tool.* Modelling and Simulation in Materials Science and Engineering, 2009. **18**(1): p. 015012.
41. Zhang, S., et al., *Investigating the influence of wall frictions on hopper flows.* Granular Matter, 2014. **16**(6): p. 857-866.
42. Perge, C., et al., *Evolution of pressure profiles during the discharge of a silo.* Physical Review E, 2012. **85**(2).
43. Anand, A., et al., *Predicting discharge dynamics from a rectangular hopper using the discrete element method (DEM).* Chemical Engineering Science, 2008. **63**(24): p. 5821-5830.
44. Tian, Y., et al., *Implementing discrete element method for large-scale simulation of particles on multiple GPUs.* Computers & Chemical Engineering, 2017. **104**: p. 231-240.
45. Johnson, K.L., *contact mechanics*. 1987, London: cambridge university press.
46. Cundall, P.A. and O.D.L. Strack, *A Discrete Numerical-Model for Granular Assemblies - Reply.* Geotechnique, 1980. **30**(3): p. 335-336.
47. Allen, M.P. and D.J. Tildesley, *Computer simulation of liquids*. 1989: Oxford university press.
48. Jin, Y. and H.A. Makse, *A first-order phase transition defines the random close packing of hard spheres.* Physica A Statistical Mechanics & Its Applications, 2010. **389**(23): p. 5362-5379.
49. Aste, T., M. Saadatfar, and T.J. Senden, *Geometrical structure of disordered sphere packings.* Physical Review E, 2005. **71**(6): p. 061302.
50. Wang, S., et al., *Simulation of flow behavior of liquid and particles in a liquid-solid fluidized bed.* Powder Technology, 2012. **224**: p. 365-373.
51. Dommelen, B.L.V., *Physical interpretation of the virial stress.* 2003.

Figures

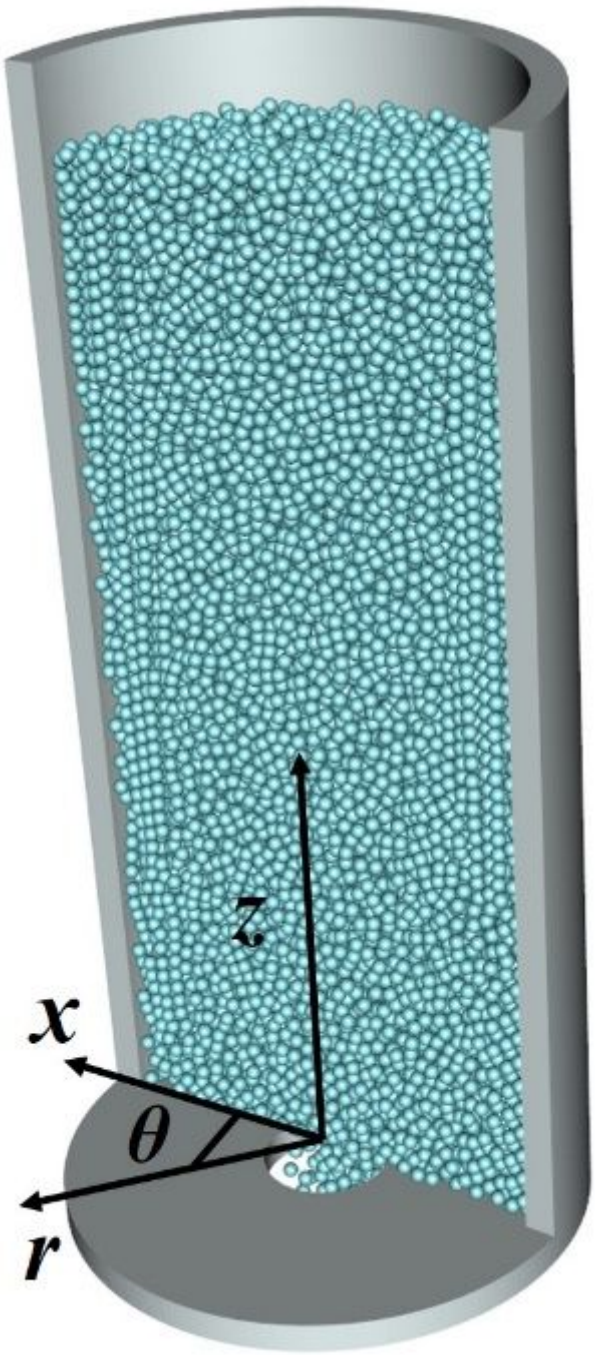

Figure 1

The simulation system with a cylindrical coordinates system. The origin is set at the center of the bottom.

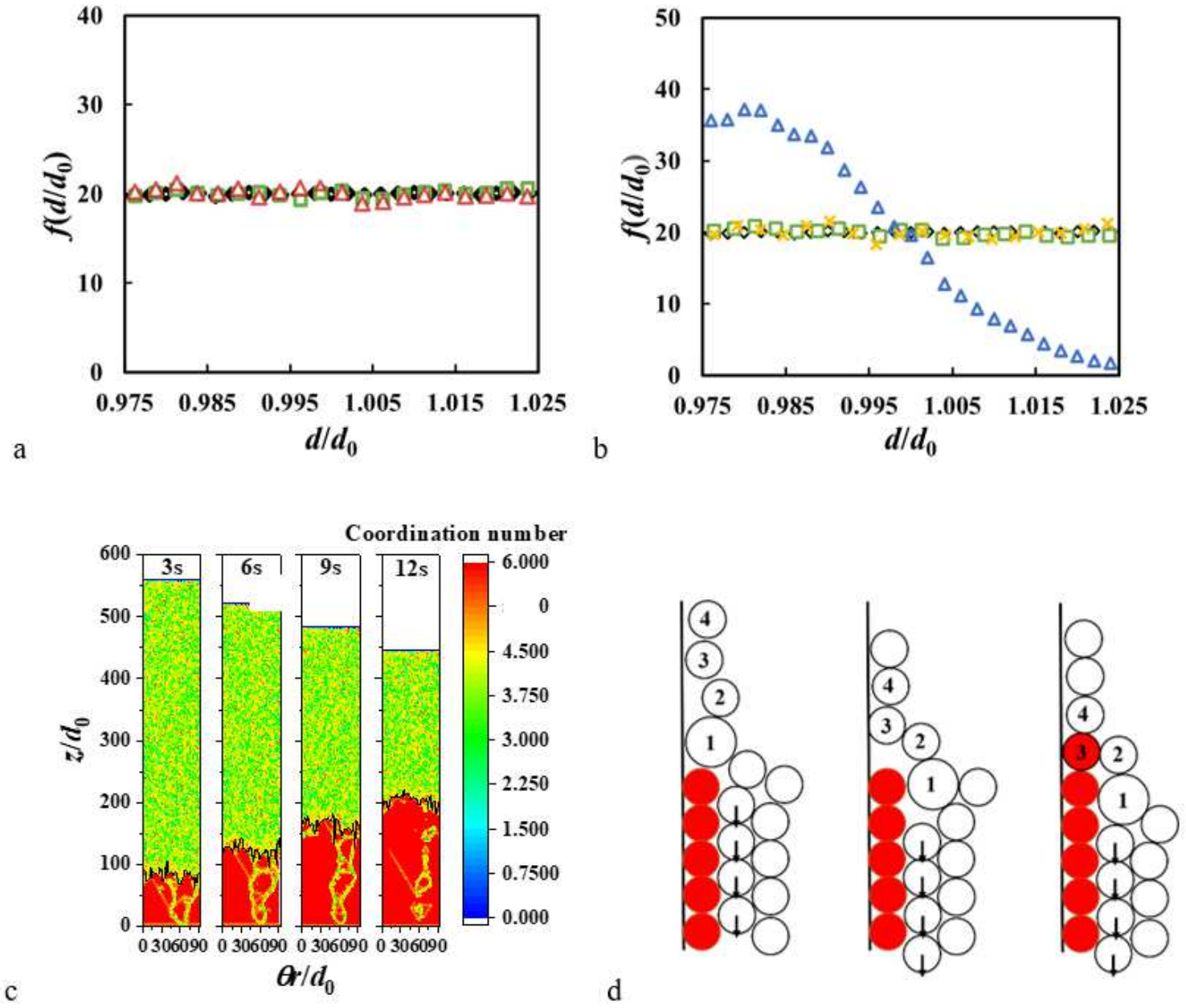

Figure 2

a) Frequency distribution of the initial radial coordination of shell particles. Size distribution of different particle groups with a) μpp=0.5; b) μpp=0.05. Diamond(black): all particles in the hopper. Square(green): particles at the boundary when the flow starts. Upper triangle(blue): the shell particles when the drainage is over. x(yellow): the boundary particles above the upper surface during the drainage. Upper triangle(red): the boundary particles when flow is stable. c) Side area of the cylindrical hopper at different time (3, 6, 9, 12s after the flow starts), showing the growth of the crystallized shell. The color denotes the coordination number of wall particles. The red particles are shell particles. Black lines denote the local surface of the shell. d) Illustration of the shell growth. The red particles denote the shell particles. The proper size particle (particle 3) is selected by settling down process while particles 1 and 2 flow aside.

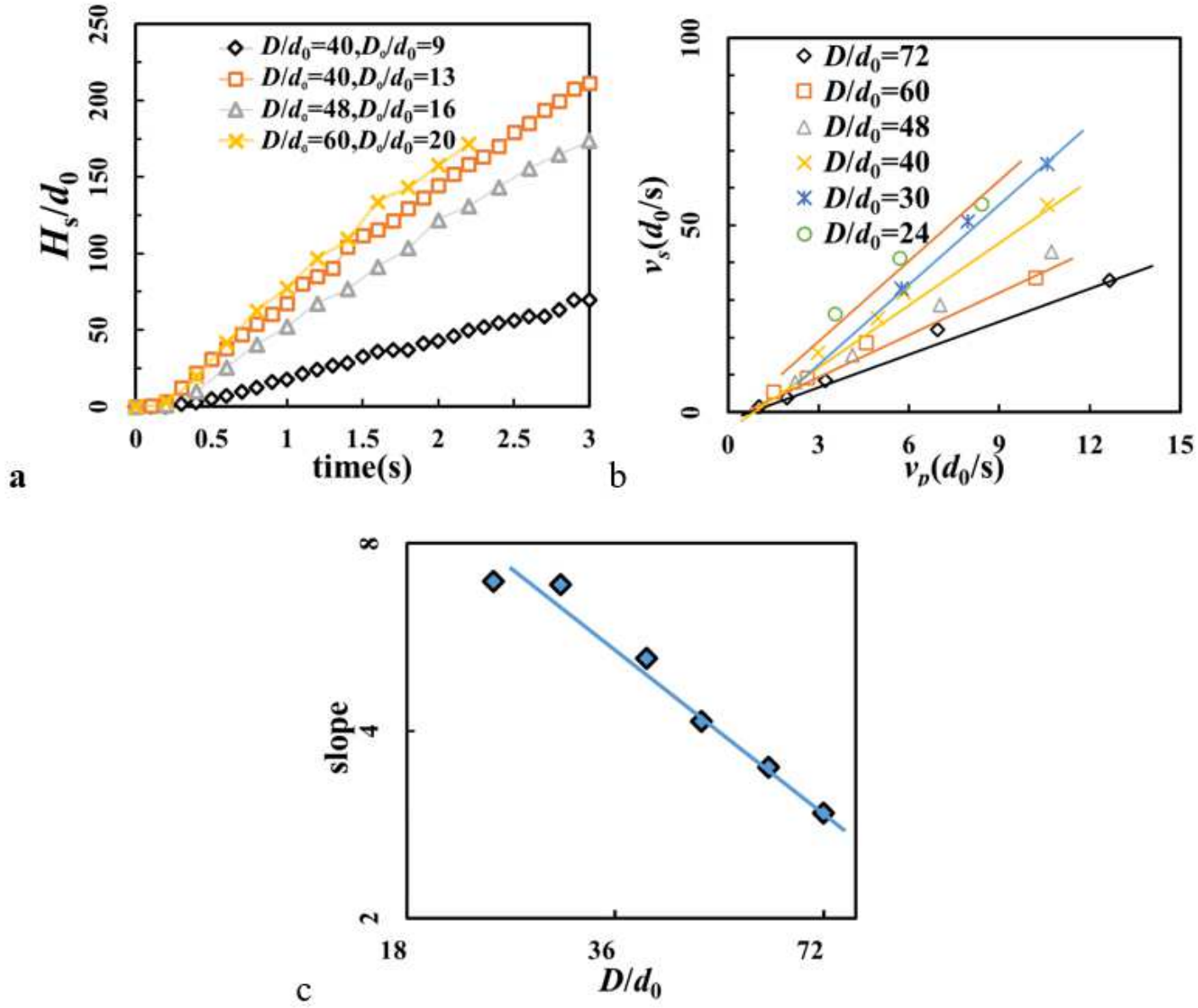

Figure 3

a) The development of averaged shell surface height (Hs) with different D and D0. b) The relation between vp and vs. c) Log-log plot of the slope of the linear relationship presented in Figure 4b. Here λ=0.

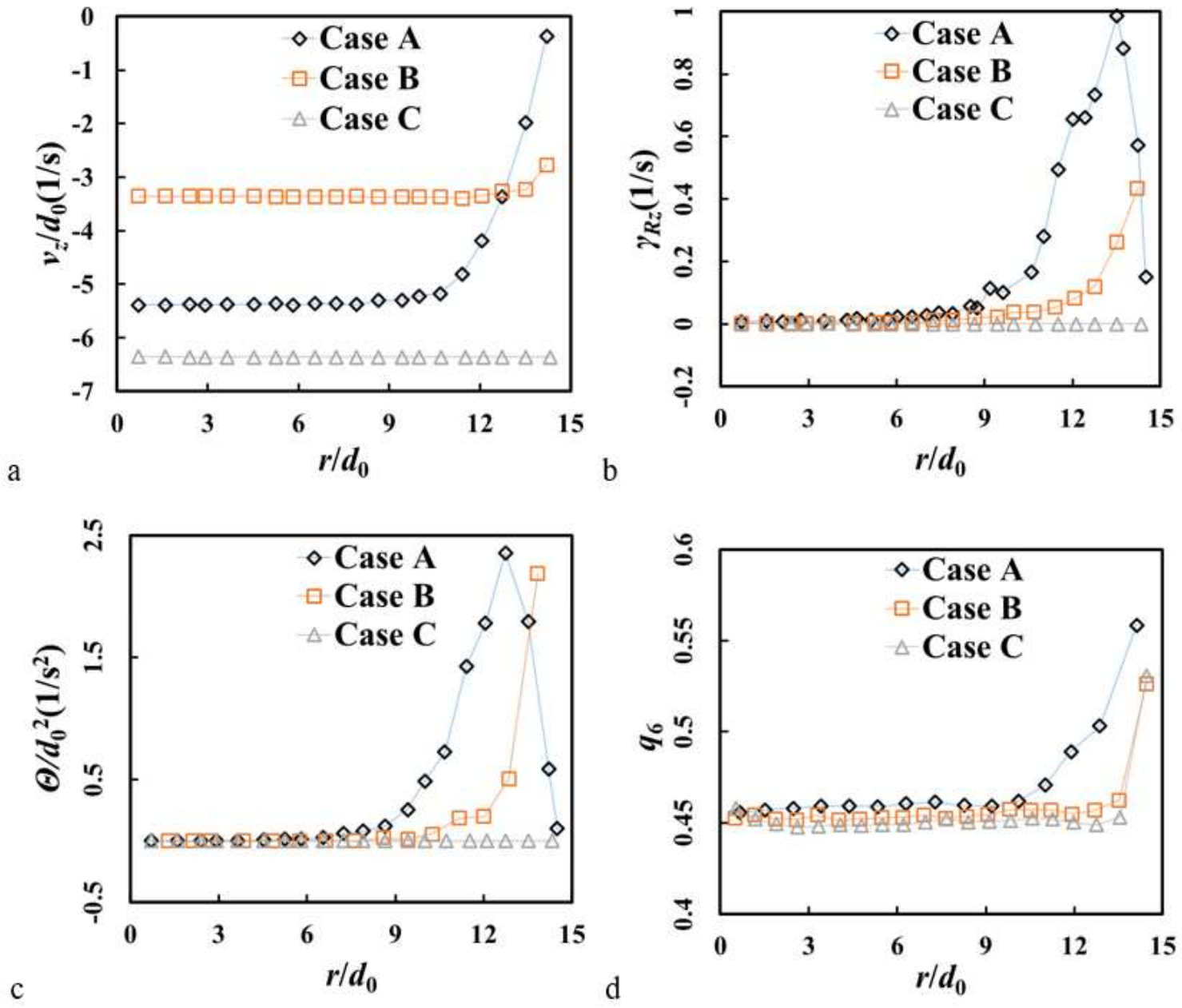

Figure 4

Radial profiles of a) vertical velocity vz, b) shear rate, c) granular temperature, d) orientational order q6 at z=100 d0.

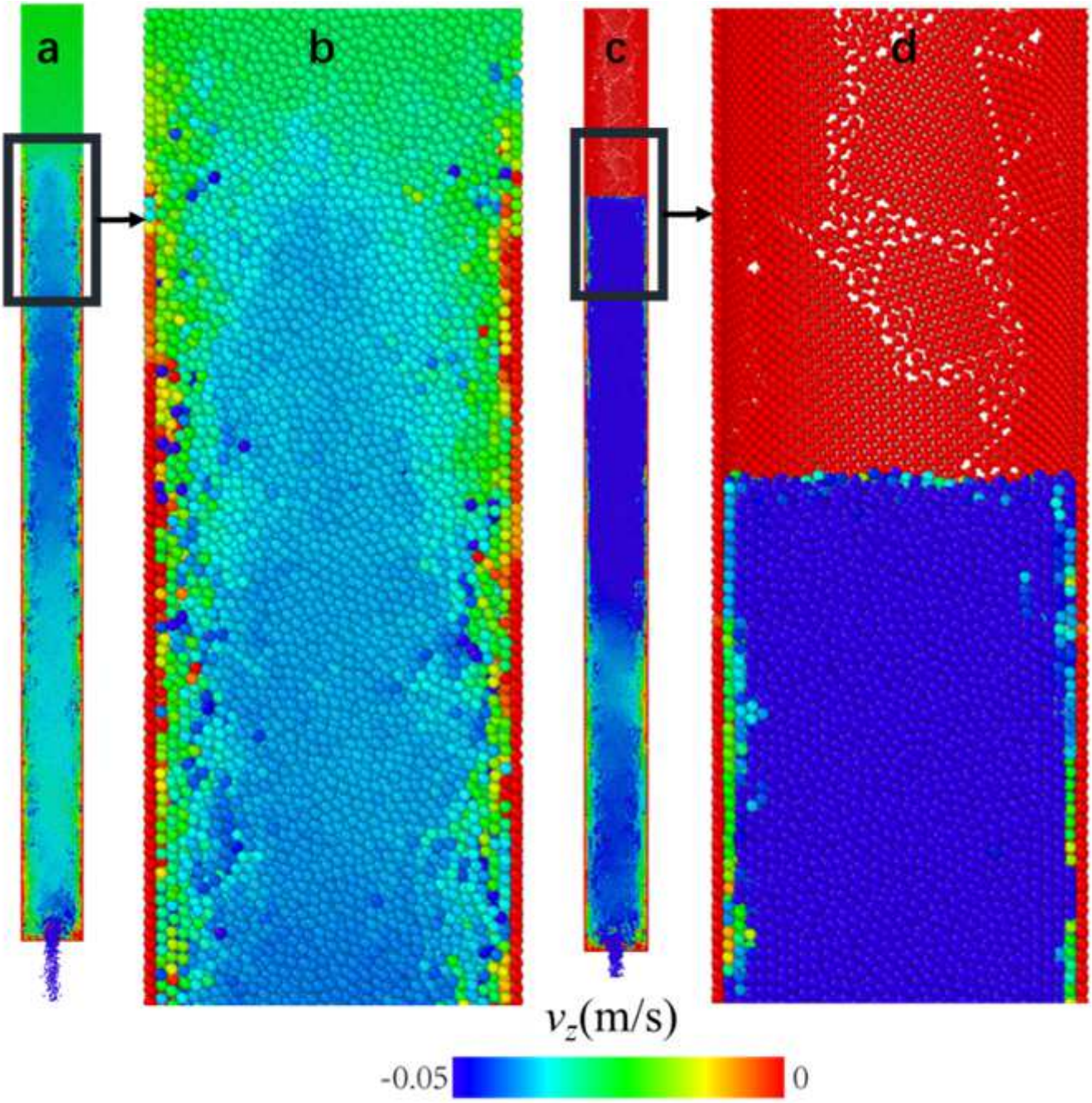

Figure 5

a) A cross section of the flow at a stage when the crystallized shell does not reach the descending top surface. b) Enlarged picture of the part around the growing shell surface in a). c) The cross section of the flow when the top surface level is below the shell surface. d) Enlarged picture of the part around the top surface in c), with the developed shell reaching well above the surface. The results in this figure is visualized by [40].

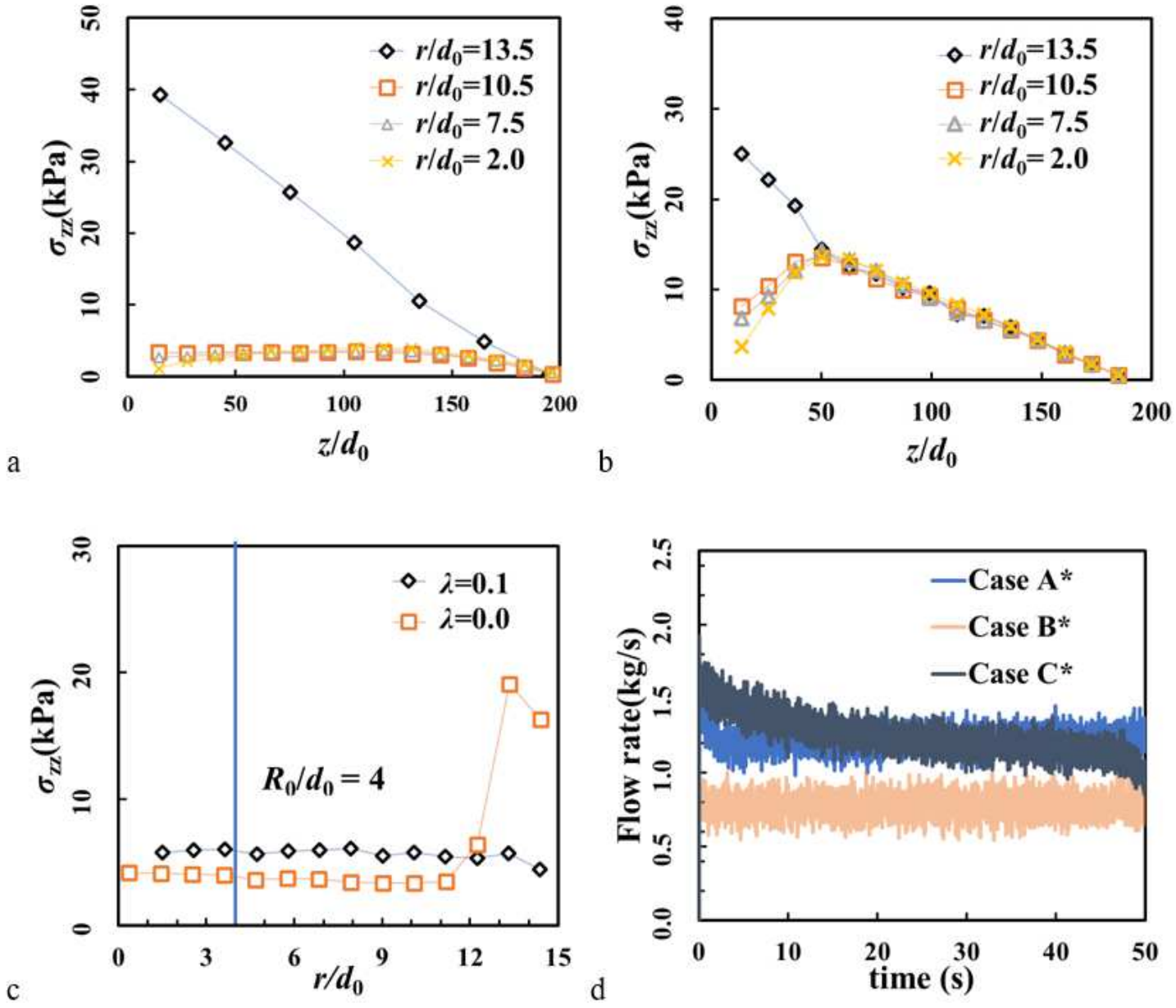

Figure 6

Vertical stress σzz along z axis in a) Case A* (λ=0) and b) in Case C* (λ=0.1) (see Table 2). c) σzz in the radial direction at z/d0 =100. The vertical line marks the radius of outlet. d) Temporal profile of instantaneous mass flow rate in Cases A*, B* and C*.

Supplementary Files

This is a list of supplementary files associated with this preprint. Click to download.

- supplementary.docx
- video1.avi

- video2.avi
- video3.avi